A population-level invasion by transposable elements in a fungal pathogen

Ursula Oggenfuss[1], Thomas Badet[1], Thomas Wicker[2], Fanny E. Hartmann[3,4], Nikhil K. Singh[1], Leen N. Abraham[1], Petteri Karisto[4,6], Tiziana Vonlanthen[4], Christopher C. Mundt[5], Bruce A. McDonald[4], Daniel Croll[1,*]

[1] Laboratory of Evolutionary Genetics, Institute of Biology, University of Neuchâtel, 2000 Neuchâtel, Switzerland
[2] Institute for Plant and Microbial Biology, University of Zurich, Zurich, Switzerland
[3] Ecologie Systématique Evolution, Bâtiment 360, Univ. Paris-Sud, AgroParisTech, CNRS, Université Paris-Saclay, 91400 Orsay, France
[4] Plant Pathology, Institute of Integrative Biology, ETH Zurich, Zurich, Switzerland
[5] Department of Botany and Plant Pathology, Oregon State University, Corvallis, OR 97331-2902, USA
[6] Department of Evolutionary Biology and Environmental Studies, University of Zurich, Zurich, Switzerland

[*] Author for correspondence: daniel.croll@unine.ch

Data availability: Sequence data is deposited on the NCBI Short Read Archive under the accession numbers PRJNA327615, PRJNA596434 and PRJNA178194.

Author contributions: UO and DC conceived the study, UO, TW and DC designed analyses, UO, TB and TV performed analyses, FEH, NKS, LNA, PK, CCM and BAM provided samples/datasets, BAM and DC provided funding, UO and DC wrote the manuscript with input from co-authors. All authors reviewed the manuscript and agreed on submission.

ABSTRACT

Transposable elements (TEs) are key drivers of adaptive evolution within species. Yet, the propagation of TEs across the genome can be highly deleterious and ultimately lead to genome expansions. Hence, TE activity is likely under complex selection regimes within species. To address this, we analyzed a large whole-genome sequencing dataset of the fungal wheat pathogen *Zymoseptoria tritici* harboring TE-mediated adaptations to overcome host defenses and fungicides. We built a robust map of genome-wide TE insertion and deletion loci for six populations and 284 fungal individuals across the world. We identified a total of 2'456 unfixed TE loci within the species and a significant excess of rare insertions indicating strong purifying selection. A subset of TEs recently swept to near complete fixation with at least one locus likely contributing to higher levels of fungicide resistance. TE-driven adaptation was also supported by evidence for selective sweeps. In parallel, we identified a substantial genome-wide expansion of TE families from the pathogen's center of origin to more recently founded populations, suggesting that population bottlenecks played a major role in shaping TE content of the genome. The most dramatic expansion occurred among a pair of North American populations collected in the same field at an interval of 25 years. We show that both the activation of specific TEs and relaxed purifying selection likely underpin the expansion. Our study disentangles the effects of selection and TE bursts leading to intra-specific genome expansions, providing a model to recapitulate TE-driven genome evolution over deeper evolutionary timescales.

INTRODUCTION

Transposable elements (TEs) are mobile repetitive DNA sequences with the ability to independently insert into new regions of the genome. TEs are major drivers of genome instability and epigenetic change (Eichler & Sankoff, 2003). Insertion of TEs can disrupt coding sequences, trigger chromosomal rearrangements, or alter expression profiles of adjacent genes (Lim, 1988; Petrov *et al.*, 2003; Slotkin & Martienssen, 2007; Hollister & Gaut, 2009; Oliver *et al.*, 2013). Hence, TE activity can have phenotypic consequences and impact host fitness. While TE insertion dynamics are driven by the selfish interest for proliferation, the impact on the host can range from beneficial to highly deleterious. For instance, TE insertions were shown to cause upregulation of genes influencing coloration and cold adaptation of fruits (Butelli *et al.*, 2012; Zhang *et al.*, 2019). The most dramatic examples of TE insertions underpinned rapid adaptation of populations or species (Feschotte, 2008; Chuong *et al.*, 2017), particularly following drastic environmental changes or colonization events. In the peppered moth, a TE insertion into an intron caused a darker phenotype, which provided better camouflage on tree bark darkened by pollution (van't Hof *et al.*, 2016). In *Drosophila melanogaster*, developmental timing adapted after migration to North America based on TE-mediated up-regulation of juvenile hormone production (González *et al.*, 2009). However, many studies indicate that the fate of TEs in populations is largely determined by purifying selection (Rizzon *et al.*, 2003; Walser *et al.*, 2006; Cridland *et al.*, 2013; Stuart *et al.*, 2016; Lai *et al.*, 2017; Stritt *et al.*, 2017). Thus, the broad range of fitness outcomes associated with individual TE insertions suggests that populations are likely to evolve complex selection regimes to constrain the transposition activity of TEs.

The fate of a new TE insertion in a population is dependent on the joint impact of selection and demography. TE insertions that have deleterious effects should be under strong purifying selection and are expected to be purged quickly from populations (Blumenstiel *et al.*, 2014). TE insertions with neutral effects on host fitness are governed by genetic drift alone. Hence, neutral TE insertion frequencies can fluctuate according to the strength of drift and historical bottlenecks. Effective

population size becomes crucial to determine these dynamics and TEs may reach fixation with a high probability in small populations (Jurka *et al.*, 2011). Low frequency TEs tend to be young or slightly deleterious insertions while high frequency TEs tend to be old insertions (Barron *et al.*, 2014). Beneficial TEs are expected to experience strong positive selection and rapid fixation such as observed for the dark phenotype in the peppered moth (Barron *et al.*, 2014) (van't Hof *et al.*, 2016). In addition to negative selection against newly inserted TEs, genomic defense mechanisms can directly disable transposition activity. Across eukaryotes, epigenetic silencing is a shared defense mechanism against TEs (Slotkin & Martienssen, 2007). Fungi evolved an additional and highly specific defense system introducing repeat-induced point (RIP) mutations into any nearly identical set of sequences. TE control by RIP and RIP-like mechanisms shows a patchy distribution across the fungal tree of life and may carry significant costs, including occasional leakage of RIP into adjacent regions (Galagan & Selker, 2004; Rouxel *et al.*, 2011). Thus, the spread of TEs across the genome and the population-level frequencies at individual TE loci will be governed by a complex set of factors. However, the relative importance of demography, selection and genomic defenses on TE dynamics remains poorly understood.

A crucial property predicting the invasion success of TEs in a genome is the transposition rate. TEs mostly expand through family-specific bursts of transposition followed by prolonged phases of transposition inactivity. Bursts of insertions of different retrotransposon families were observed across eukaryotic lineages including *Homo sapiens*, *Zea mays*, *Oryza sativa* and *Blumeria graminis* (Shen *et al.*, 1991; SanMiguel *et al.*, 1998; Eichler & Sankoff, 2003; Lu *et al.*, 2017; Frantzeskakis *et al.*, 2018). Prolonged bursts without effective counter-selection are thought to underpin genome expansion. In the symbiotic fungus *Cenococcum geophilum*, the burst of TEs resulted in a dramatically expanded genome compared to closely related species (Peter *et al.*, 2016). Similarly, a burst of a TE family in brown hydras led to an approximately three-fold increase of the genome size compared to related hydras (Wong *et al.*, 2019). Across the tree of life, genome sizes vary by multiple orders of magnitude and enlarged genomes are invariably colonized by TEs (Kidwell, 2002). Population size variation is among the few correlates of genome size across major groups,

suggesting that the efficacy of selection plays an important role in controlling TE activity (Lynch, 2007). Reduced selection efficacy against deleterious TE insertions is expected to lead to a ratchet-like increase in genome size. TE-rich, enlarged genomes often show an isochore structure alternating gene-rich and TE-rich regions (Rouxel *et al.*, 2011). Genomic compartments rich in TEs often harbor genes showing high variability and may harbor rapidly evolving genes such as effectors in pathogens or resistance genes in plants (Raffaele & Kamoun, 2012; Jiao & Schneeberger, 2019). Hence, incipient genome expansions are likely driven by population-level processes such as TE insertion dynamics, strength of selection and demography.

The fungal wheat pathogen *Zymoseptoria tritici* recently gained major TE-mediated adaptations to colonize host plants and tolerate environmental and agricultural stress (Omrane *et al.*, 2015, 2017; Krishnan *et al.*, 2018; Meile *et al.*, 2018). Clusters of TEs are often associated with genes encoding important pathogenicity functions (*i.e.* effectors), recent gene gains or losses (Hartmann & Croll, 2017), and major chromosomal rearrangements (Croll *et al.*, 2013; Plissonneau *et al.*, 2016). Transposition activity of TEs also had a genome-wide impact on gene expression profiles during infection (Fouché *et al.*, 2019). The compact genome of ~39 Mb is completely assembled and contains ~17% TEs (Goodwin *et al.*, 2011; Dhillon *et al.*, 2014). The well-characterized demographic history of the pathogen and evidence for recent TE-mediated adaptations make *Z. tritici* an ideal model to recapitulate the process of TE insertion dynamics, adaptive evolution and changes in genome size at the population level.

We aimed to retrace the population-level context of TE insertion dynamics across the species range by analyzing six populations sampled on four continents for a total of 284 genomes. We first aimed to develop a robust pipeline to detect newly inserted TEs using short read sequencing datasets. Then, we tested for the strength of purifying selection against TE insertions within and across populations. In addition, we searched for signatures of adaptive evolution driven by TE activity across populations. Using knowledge of the colonization history of the pathogen, we analyzed whether population bottlenecks were associated with substantial changes in the TE content of individual

genomes. In particular, we tested whether geographically isolated populations experienced distinct bursts of TEs.

METHODS

FUNGAL ISOLATE COLLECTION AND SEQUENCING

We analyzed 295 *Z. tritici* isolates covering six populations originating from four geographic locations and four continents (Supplementary Table S1), including: Middle East 1992 (*n* = 30 isolates, Nahal Oz, Israel), Australia 2001 (*n* = 27, Wagga Wagga), Europe 1999 (*n* = 33, Berg am Irchel, Switzerland), Europe 2016 (*n* = 52, Eschikon, ca. 15km from Berg am Irchel, Switzerland), North America 1990 and 2015 (*n* = 56 and *n* = 97, Willamette Valley, Oregon, United States) (McDonald *et al.*, 1996; Linde *et al.*, 2002; Zhan *et al.*, 2002, 2003, 2005). Illumina short read data from the Middle East, Australia, European 1999 and North American 1990 populations were obtained from the NCBI Short Read Archive under the BioProject PRJNA327615 (Hartmann *et al.*, 2017). For, the Switzerland 2016 and Oregon 2015 populations, asexual spores were harvested from infected wheat leaves from naturally infected fields and grown in YSB liquid media including 50 mgL^{-1} kanamycin and stored in silica gel at −80°C. High-quality genomic DNA was extracted from liquid cultures using the DNeasy Plant Mini Kit from Qiagen (Venlo, Netherlands). The isolates were sequenced on an Illumina HiSeq in paired-end mode and raw reads were deposited on the NCBI Short Read Archive under the BioProject PRJNA596434.

TE INSERTION DETECTION

The quality of Illumina short reads was determined with FastQC version 0.11.5 (Figure 1A) (Andrews *et al.*, 2013). To remove spuriously sequenced Illumina adaptors and low quality reads, we trimmed the sequences with Trimmomatic version 0.36, using the following filter parameters: illuminaclip:TruSeq3-PE-2.fa:2:30:10 leading:10 trailing:10 slidingwindow:5:10 minlen:50 (Bolger *et al.*, 2014). We created repeat sequence consensi for TE families (Supplementary File S1) in the

complete reference genome IPO323 (Goodwin *et al.*, 2011) with RepeatModeler version open-4.0.7 based on the RepBase Sequence Database (Smit & Hubley; Bao *et al.*, 2015). TE classification into superfamilies and families was based on an approach combining detection of conserved protein sequences and tools to detect non-autonomous TEs (Badet *et al.*, 2019). To detect TE insertions, we used the R-based tool ngs_te_mapper version 79ef861f1d52cdd08eb2d51f145223fad0b2363c integrated into the McClintock pipeline version 20cb912497394fabddcdaa175402adacf5130bd1, using bwa version 0.7.4-r385 to map Illumina short reads, samtools version 0.1.19 to convert alignment file formats and R version 3.2.3 (Li & Durbin, 2009; Li *et al.*, 2009; Linheiro & Bergman, 2012; Nelson *et al.*, 2017; R Core Team, 2017).

DOWN-SAMPLING ANALYSIS

We performed a down-sampling analysis to estimate the sensitivity of the TE detection with ngs_te_mapper based on variation in read depth. We selected one isolate per population matching the average coverage of the population. We extracted the per-base pair read depth with the genomecov function of bedtools version 2.27.1 and calculated the genome-wide mean read depth (Quinlan & Hall, 2010). The number of reads in the original fastq file was reduced in steps of 10% to simulate the impact of reduced coverage. We analyzed each of the obtained reduced read subsets with ngs_te_mapper using the same parameters as described above. The correlation between the number of detected insertions and the read depth was visualized using the function nls with model SSlogis in R, (Wickham, 2016). The number of detected TEs increased with the number of reads until reaching a plateau indicating saturation (Figure 1B). Saturation was reached at a coverage of approximately 15X, hence we retained only isolates with an average read depth above 15X for further analyses. We thus excluded one isolate from the Oregon 2015 population and ten isolates from the Switzerland 2016 population.

187 VALIDATION PROCEDURE FOR PREDICTED TE INSERTIONS

188 ngs_te_mapper detects the presence but not the absence of a TE at any given locus. We devised
189 additional validation steps to ascertain both the presence as well absence of a TE across all loci in all
190 individuals. For TE loci with missing information about presence or absence, we conducted further
191 analyses. TEs absent in the reference genome were validated by re-analyzing mapped Illumina reads.
192 Reads spanning both parts of a TE sequence and an adjacent chromosomal sequence should only
193 map to the reference genome sequence and cover the target site duplication (TSD) of the TE (Figure
194 1C). We used bowtie2 version 2.3.0 with the parameter --very-sensitive-local to map Illumina short
195 reads of each isolate on the reference genome IPO323 (Langmead & Salzberg, 2012). Mapped
196 Illumina short reads were then sorted and indexed with samtools and the resulting bam file was
197 converted to a bed file with the function bamtobed in bedtools. We extracted all mapped reads with
198 an end point located within 100 bp of the TSD (Figure 1C). We tested whether the number of reads
199 with a mapped end around the TSD significantly deviated if the mapping ended exactly at the
200 boundary. A mapped read ending exactly at the TSD boundary is indicative of a split read mapping
201 to a TE sequence not present in the reference genome. To test for the deviation in the number of read
202 mappings around the TSD, we used a Poisson distribution and the *ppois* function in R version 3.5.1
203 (Figure 1C). We identified a TE as present in an isolate if tests on either side of the TSD had a *p*-
204 value < 0.001 (Supplementary Table S1, S2, Figure S1B).
205
206 For TEs present in the reference genome, we analyzed evidence for spliced junction reads spanning
207 the region containing the TE. Spliced reads are indicative of a discontinuous sequence and, hence,
208 absence of the TE in a particular isolate (Figure 1D). We used STAR version 2.5.3a to detect spliced
209 junction reads with the following set of parameters: --runThreadN 1 --outFilterMultimapNmax 100 -
210 -winAnchorMultimapNmax 200 --outSAMmultNmax 100 --outSAMtype BAM Unsorted --
211 outFilterMismatchNmax 5 --alignIntronMin 150 --alignIntronMax 15000 (Dobin *et al.*, 2012). We
212 then sorted and indexed the resulting bam file with samtools and converted split junction reads with
213 the function bam2hints in bamtools version 2.5.1 (Barnett *et al.*, 2011). We selected loci without
214 overlapping spliced junction reads using the function intersect in bedtools with the parameter -loj -v.

We considered a TE as truly absent in an isolate if ngs_te_mapper did not detect a TE and no evidence for spliced junction reads were found. If the absence of a TE could not be confirmed by spliced junction reads, we labelled the genotype as missing. Finally, we excluded TE loci with more than 20% missing data from further investigations (Figure 1D and Supplementary Figure S1C).

Clustering of TE insertions into loci

We identified insertions across isolates as being the same locus if all detected TEs belonged to the same TE family and insertion sites differed by ≤100 bp (Supplementary Figure S2). We used the R package *GenomicRanges* version 1.28.6 with the functions makeGRangesFromDataFrame and findOverlaps and the R package *devtools* version 1.13.4 (Lawrence *et al.*, 2013; Wickham & Chang, 2016). We used the R package *dplyr* version 0.7.4 to summarize datasets (Wickham *et al.*, 2017). Population-specific frequencies of insertions were calculated with the function allele.count in the R package *hierfstat* version 0.4.22 (Goudet & Jombart, 2015). We conducted a principal component analysis for TE insertion frequencies filtering for a minor allele frequency ≥ 5%. We also performed a principal component analysis for genome-wide single nucleotide polymorphism (SNP) data obtained from Hartmann et al (2017). As described previously, SNPs were hard-filtered with VariantFiltration and SelectVariants tools integrated in the Genome Analysis Toolkit (GATK) (McKenna *et al.*, 2010). SNPs were removed if any of the following filter conditions applied: QUAL<250; QD<20.0; MQ<30.0; -2 > BaseQRankSum > 2; -2 > MQRankSum > 2; -2 > ReadPosRankSum > 2; FS>0.1. SNPs were excluded with vcftools version 0.1.17 and plink version 1.9 requiring a genotyping rate >90% and a minor allele frequency >5% (https://www.cog-genomics.org/plink2, Chang et al., 2015). Finally, we converted tri-allelic SNPs to bi-allelic SNPs by recoding the least frequent allele as a missing genotype. Principal component analysis was performed using the *gdsfmt* and *SNPRelate* packages in R (Zheng *et al.*, 2012, 2017). For a second principal component analysis with a reduced set of random markers, we randomly selected SNPs with vcftools and the following set of parameters: --maf 0.05 –thin 200'000 to obtain an approximately equivalent number of SNPs as TE loci.

242

243 GENOMIC LOCATION OF TE INSERTIONS

244 To characterize the genomic environment of TE insertion loci, we split the reference genome into
245 non-overlapping windows of 10 kb using the function splitter from EMBOSS version 6.6.0 (Rice *et*
246 *al.*, 2000). TEs were located in the reference genome using RepeatMasker providing consensi from
247 *RepeatModeler Open-1.0* (Smit & Hubley; http://www.repeatmasker.org). To analyze coding
248 sequence, we retrieved the gene annotation for the reference genome (Grandaubert *et al.*, 2015). We
249 estimated the percentage covered by genes or TEs per window using the function intersect in
250 bedtools. Additionally, we calculated the GC content using the tool get_gc_content
251 (https://github.com/spundhir/RNA-Seq/blob/master/get_gc_content.pl). We also extracted the
252 number of TEs present in 1 kb windows up- and downstream of each annotated gene with the
253 function window in bedtools with the parameters -l 1000 -r 1000 and calculated the relative
254 distances with the closest function in bedtools. For the TEs inserted into genes, we used the intersect
255 function in bedtools to distinguish intron and exon insertions with the parameters -wo and -v,
256 respectively. For each 100 bp segment in the 1kb windows as well as for introns and exons, we
257 calculated the mean number of observed TE insertions per base pair.

258

259 POPULATION DIFFERENTIATION IN TE FREQUENCIES

260 We calculated Nei's fixation index (F_{ST}) between pairs of populations using the R packages *hierfstat*
261 and *adegenet* version 2.1.0 (Jombart, 2008; Jombart & Ahmed, 2011). To understand the
262 chromosomal context of TE insertion loci across isolates, we analyzed draft genome assemblies. We
263 generated *de novo* genome assemblies for all isolates using SPAdes version 3.5.0 with the parameter
264 --careful and a kmer range of "21, 29, 37, 45, 53, 61, 79, 87" (Bankevich *et al.*, 2012). We used
265 blastn to locate genes adjacent to TE insertion loci on genomic scaffolds of each isolate. We then
266 extracted scaffold sequences surrounding 10 kb up- and downstream of the localized gene with the
267 function faidx in samtools and reverse complemented the sequence if needed. Then, we performed
268 multiple sequence alignments for each locus across all isolates with MAFFT version 7.407 with

parameter --maxiterate 1000 (Katoh & Standley, 2013). We performed visual inspections to ensure correct alignments across isolates using Jalview version 2.10.5 (Waterhouse *et al.*, 2009). To generate phylogenetic trees of individual gene or TE loci, we extracted specific sections of the alignment using the function extractalign in EMBOSS and converted the multiple sequence alignment into PHYLIP format with jmodeltest version 2.1.10 using the -getPhylip parameter. We then estimated maximum likelihood phylogenetic trees with the software PhyML version 3.0, the K80 substitution model and 100 bootstraps on the ATGC South of France bioinformatics platform (Guindon & Gascuel, 2003; Guindon *et al.*, 2010; Darriba *et al.*, 2012). Bifurcations with a supporting value lower than 10% were collapsed in TreeGraph version 2.15.0-887 beta and trees were visualized as circular phylograms in Dendroscope version 2.7.4 (Huson *et al.*, 2007; Stöver & Müller, 2010). For loci showing complex rearrangements, we generated synteny plots using 19 completely sequenced genomes from the same species using the R package *genoplotR* version 0.8.9 (Guy *et al.*, 2010; Badet *et al.*, 2019).

We analyzed signatures of selective sweeps using the extended haplotype homozygosity (EHH) tests (Sabeti *et al.*, 2007) implemented in the R package REHH (Gautier & Vitalis, 2012). We analyzed within-population signatures based on the iHS statistic and chose a maximum gap distance of 20 kb. We also analyzed cross-population EHH (XP-EHH) signatures testing the following two population pairs: North America 1990 versus North America 2015, Europe 1999 versus Europe 2016. We defined significant selective sweeps as being among the 99.9th percentile outliers of the iHS and XP-EHH statistics. Significant SNPs at less than 5 kb were clustered into a single selective sweep region adding +/- 2.5 kb. Finally, we analyzed whether TE loci were within 10 kb of a region identified as a selective sweep using the function intersect from bedtools.

FUNGICIDE RESISTANCE ASSAY

To quantify susceptibility towards propiconazole we performed a microtiter plate assay. Isolates were grown on yeast malt sucrose agar for five days and spores were harvested. We then tested for growth inhibition by growing spores (2.5 x 10^4 spores/ml) in Sabouraud-dextrose liquid medium

with differing concentrations of propiconazole (0.00006, 0.00017, 0.0051, 0.0086, 0.015, 0.025, 0.042, 0.072, 0.20, 0.55, 1.5 mg/L). We incubated the plates stationary in the dark at 21°C and 80% relative humidity for four days and measured optical density at 605 nm. We calculated EC_{50} with the R package *drc* (Ritz & Streibig, 2005).

RESULTS

A DYNAMIC TE LANDSCAPE SHAPED BY STRONG PURIFYING SELECTION

We analyzed 284 genomes from a worldwide set of six populations spanning the distribution range of the wheat pathogen *Z. tritici*. To ascertain the presence or absence of TEs across the genome, we developed a robust pipeline (Figure 1A) to address the fact that ngs_te_mapper is only testing for TE presence and not TE absence. In summary, we called TE insertions by identifying reads mapping both to a TE sequence and a specific location in the reference genome. Then, we assessed the minimum sequencing coverage to reliably recover TE insertions, tested for evidence of TEs using read depth at target site duplications, and scanned the genome for mapped reads indicating gaps at TE loci. We found robust evidence for a total of 18'864 TE insertions grouping into 2'465 individual loci. More than 30% of these loci have singleton TEs (Figure 2B, Supplementary Table S3). An overwhelming proportion of loci have a TE frequency below 1%. This pattern strongly supports the hypothesis that TEs actively copy into new locations but also indicates that strong purifying selection maintains nearly all TEs at low frequency (Figure 2B). We found a higher density of TE loci on accessory chromosomes, which are not shared among all isolates of the species, compared to core chromosomes (Figure 2C). This suggests relaxed selection against TE insertion on the functionally dispensable accessory chromosomes.

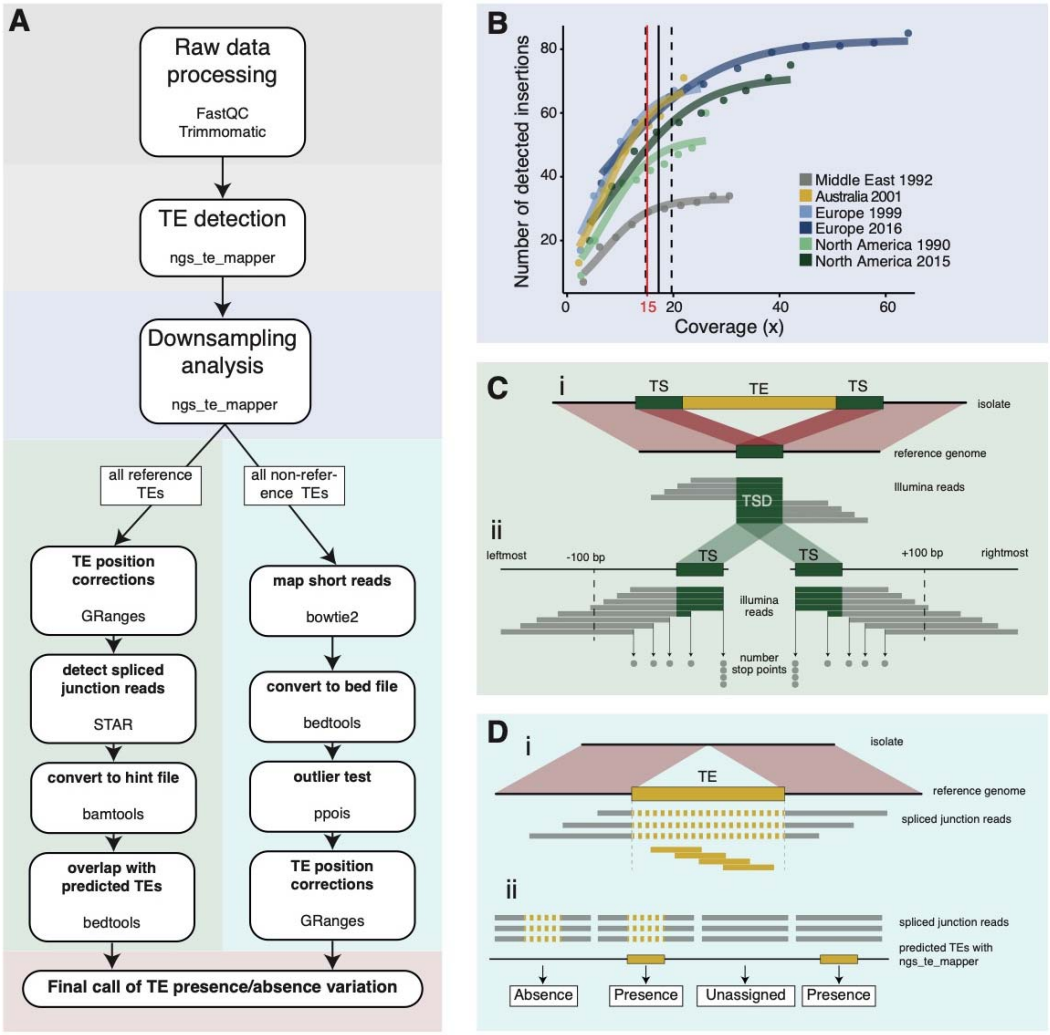

Figure 1: Overview methods and validations of transposable element (TE) insertions: (A) Bioinformatic pipeline. (B) Read depth down-sampling analysis for one isolate per population with an average coverage of the population. The vertical black line indicates the coverage at which on average 90% of the maximally detectable variants were recovered. Dashed black lines indicate the standard error. The threshold for a minimal mean coverage was set at 15X (red line). (C) Validation of insertions not present in the reference genome. (i) TE insertions that are not present in the reference genome show a duplication of the target site and the part of the reads that covers the TE will not be mapped against the reference genome. We thus expect reads to map to the TE surrounding region and the target site duplication but not the TE itself. At the target site, a local duplication of read depth is expected. (ii) We selected all reads in an interval of 100 bp up- and downstream including the target site duplication to detect deviations in the number of reads terminating near the target site duplication. (D) Validation of insertions present in the reference genome. (i) Analyses read coverage at target site duplications. (ii) Synthesis of evidence from ngs_te_mappr and split read mapping to determine TE presence or absence.

Inserted TEs grouped into 11 superfamilies and 23 families with most TEs belonging to class I/retrotransposons (*n* = 2175; Supplementary Figure S3A; Figure 2D). Most class I TEs are long terminal repeats (LTR) with 1'483 belonging to *Gypsy* superfamily (9 families in total) and 623 belonging to the *Copia* superfamily (3 families in total). We found a further 40 loci with an insertion of long interspersed repeat (LINE) elements. A total of 289 loci contain class II/DNA transposons with most belonging to Subclass 2 and order Helitron (249 loci), and to Subclass 1 (40 loci). TE families with a high total copy number across all isolates tend to also have a high copy number per genome (Figure 2E).

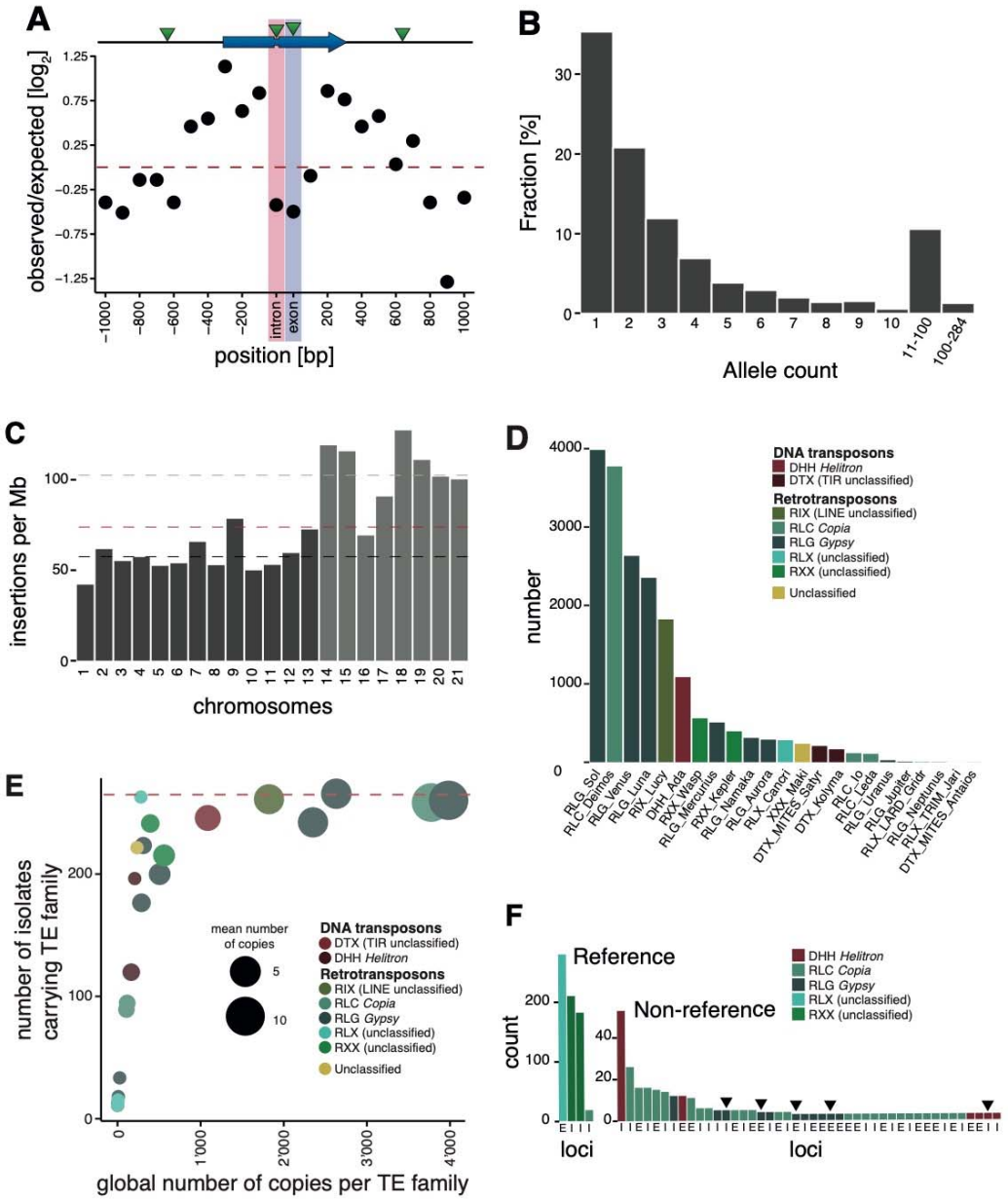

Figure 2: Transposable element (TE) landscape across populations. (A) Number of TE insertions 1 kb up- and downstream of genes on core chromosomes including introns and exons (100 bp windows). (B) Allele frequencies of the TE insertions across all isolates. (C) TE insertions per Mb on core chromosomes (dark) and accessory chromosomes (light). Dashed lines represent mean values. Red: global mean of 75.65 insertions/Mb, dark: core chromosome mean of 58.00 TEs/Mb, light: accessory chromosome mean of 102.24 insertions/Mb). (D) Number of TE insertions per family. (E) TE frequencies among isolates and copy numbers across the genome. The red line indicates the maximum number of isolates (n = 284). (F) TE insertions into introns and exons that are present in the reference genome and TEs absent from the reference genome but present in more than two copies in the populations. A hexagon indicates that the insertion was found in only one population, all other insertions were found in at least two populations. I = intron insertion, E = exon insertion.

We found 153 loci where a TE inserted into a gene, with most of these insertions being singletons (*n* = 68) or at very low frequency (Figure 2F). Overall, TE insertions into exonic sequences were less frequent than expected compared to insertions into up- and downstream regions, a pattern consistent with effective purifying selection (Figure 2A). Interestingly, insertions into introns were also strongly under-represented, likely due to the small size of most fungal introns (50-100 bp) and the high probability of disrupting splicing or adjacent coding sequences. We also found that insertions 800-1000 bp away from coding sequences of a focal gene were under-represented. Given the high gene density, with an average spacing between genes of 1,744 kb, TE insertions within 800-1000 bp of a coding gene tend to be near adjacent genes already. Taken together, TEs in the species show a high degree of transposition activity and are subject to strong purifying selection.

Detection of TE Loci under positive selection

The dynamic transposition activity can potentially generate adaptive genetic variation. To identify potentially adaptive TE insertions, we calculated the fixation index (F_{ST}) for each TE locus. Across all populations, F_{ST} was highly variable with a strong skew towards extremely low F_{ST} values (mean F_{ST}= 0.0163; Figure 3A). High F_{ST} loci tend to have high TE frequencies in either the North American population from 2015 or the Australian population. Given our population sampling, we tested for the emergence of adaptive TE insertions either in the North American or European population pairs. We selected loci having low TE insertion frequencies (< 5%) in all populations except either the North American or European population pairs, respectively (Figure 3B). We required that the locus had a TE frequencies >20% in either the 2015 North American or 2016 European population. Based on these criteria, we obtained 26 candidate loci possibly underlying local adaptation in the North American populations with 22 loci showing retrotransposon insertions, three *Helitron*, and one DNA TIR transposon (Figure 3C). In parallel, we found six loci of retrotransposons possibly underlying local adaptation in the European populations (Figure 4A and Supplementary Table S4). To further analyze evidence for TE-mediated adaptive evolution, we analyzed the whole-genome sequencing datasets for evidence of selective sweeps using selection

385 scans. Out of all 32 loci showing signatures of local adaptation in North American or European
386 populations, we found five loci overlapping selective sweep regions.
387

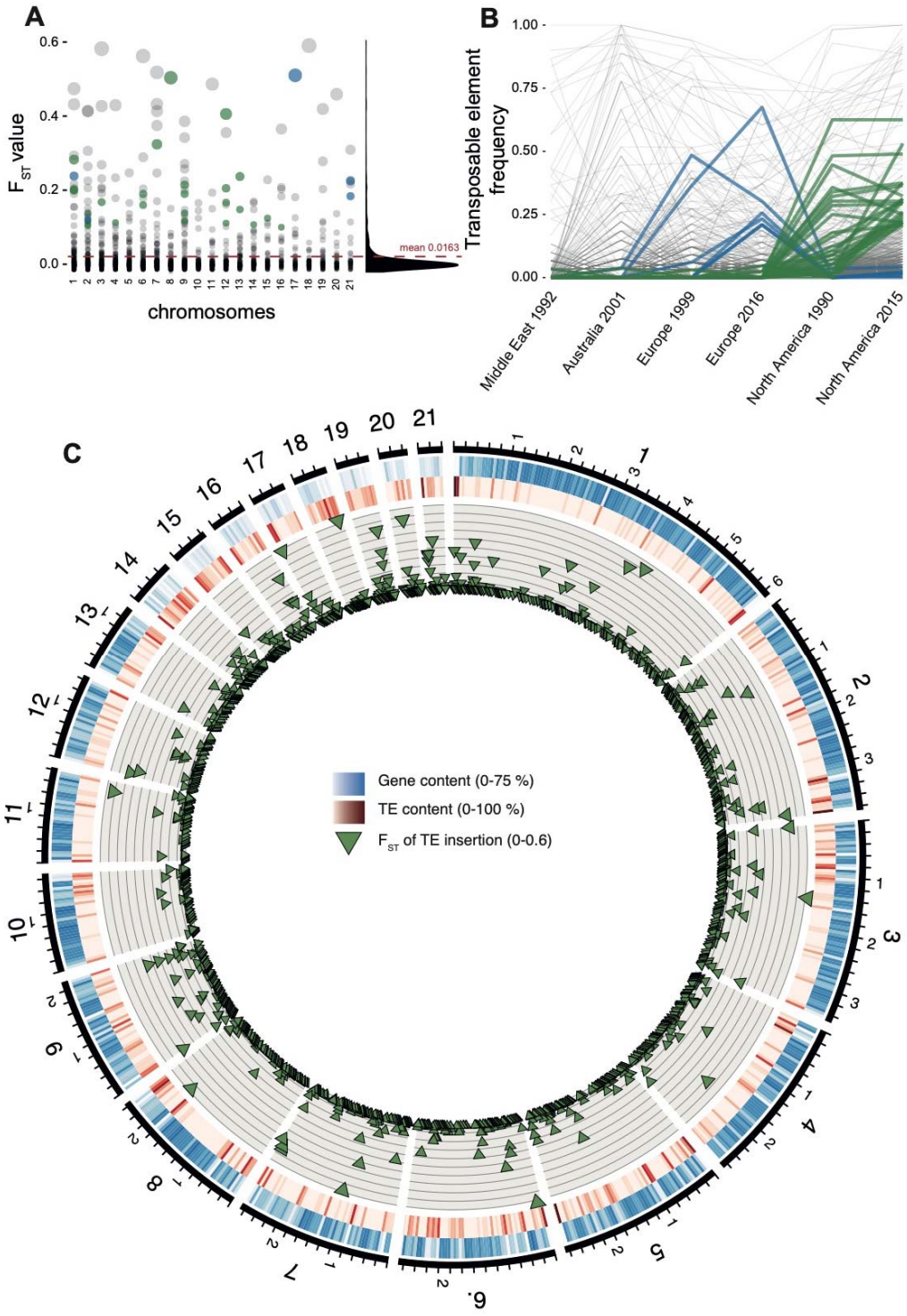

388

Figure 3: Differentiation in transposable element insertions frequencies across the genome. (A) Global pairwise F_{ST} distributions shown across the 21 chromosomes. The red horizontal line indicates the mean F_{ST} (= 0.0163). TEs with a strong frequency differences among populations are highlighted (blue: increase in Europe; green: increase in North America). (B) Allele frequency changes between the populations. Outlier TE loci are highlighted (colors as in panel A). (C) Circos plot describing from the outside to the inside: The black line indicates chromosomal position in Mb. Blue bars indicate the gene density in windows of 100 kb with darker blue representing higher gene density. Red bars indicate the TE density in windows of 100 kb with a darker red representing higher TE density. Green triangles indicate positions of TE insertions with among population F_{ST} value shown on the y-axis.

We focused on five TE insertion loci in proximity to genes with a function that can be associated to fungicide resistance or adaptation to the host. One TE insertion on chromosome 8 is only 105 bp downstream of a major facilitator superfamily (MFS) transporter gene and 644 bp upstream of a TATA box gene (Figure 4B). MFS transporters can contribute to the detoxification of antifungal compounds in the species (Omrane *et al.*, 2017). The inserted *Helitron* TE was only found in North American populations (Figure 4G). The TE insertion occurred in a gene-rich, TE-poor region and the F_{ST} = 0.51 was one of the highest values of all TE loci (Figure 4C). Generally, the *Helitron* increased strongly in copy number from the Israel to the North American populations (Figure 4D, 4F). The phylogeny of the gene encoding the MFS showed a high degree of similarity for all isolates carrying the *Helitron* insertion compared to the isolates lacking the *Helitron* (Figure 4E). This is consistent with a rapid rise in frequency of the haplotype carrying the *Helitron* driven by positive selection. Another TE locus also contains a *Helitron* of the family Ada, which was found only in the two North American populations. The TE was inserted into an intron of a Phox domain-encoding gene (Supplementary Figure S7). Phox homologous domain proteins contribute to sorting membrane trafficking (Odorizzi *et al.*, 2000). A further North American possible adaptive insertion of a *Copia* Deimos TE was 229 bp upstream of a gene encoding a SNARE domain protein and 286 bp upstream of a gene encoding a flavin amine oxidoreductase and located in a region of selective sweep (Supplementary Figure S8). SNARE domains play a role in vesicular transport and membrane fusion (Bonifacino & Glick, 2004). A TE insertion locus on chromosome 12 was both upstream 1’977 bp of a gene encoding another MFS transporter and 2’672 bp of a gene encoding an alpha/beta hydrolase fold. The inserted TE belongs to the *Gypsy* family Sol (Supplementary Figure S9). A

421 *Gypsy* Sol on chromosome 2 increased in frequency in both the North American (1.8 to 75%) as well
422 as in the European site (0 to 66.7%). This TE was inserted between a gene encoding a potential
423 virulence factor (*i.e.* an effector) and a second gene of unknown function. Interestingly, the same
424 locus contains a multitude of additional inserted TEs across populations (Supplementary Figure
425 S10). We experimentally tested whether the TE insertion loci in proximity to genes could contribute
426 to higher levels of fungicide resistance. For this, we measure growth rates of the fungal isolates in
427 the presence or absence of an azole fungicide widely deployed against the pathogen. We found that
428 the insertion of TEs at three loci was positively associated with higher levels of fungicide resistance
429 suggesting TE-mediated adaptations.
430

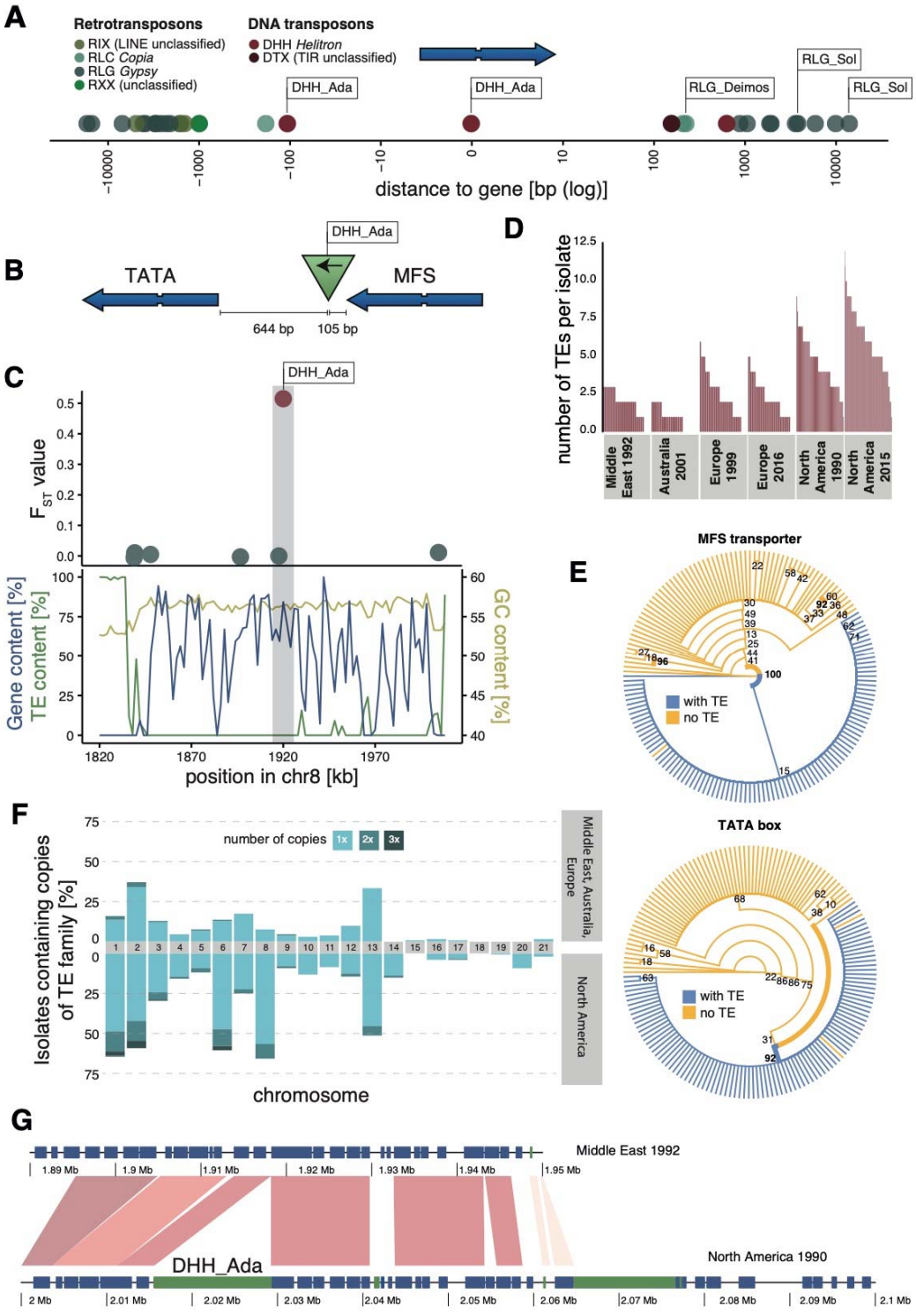

Figure 4: Candidate adaptive transposable element (TE) insertions. (A) Distribution of all extremely differentiated TEs and their distance to the closest gene. Color indicates the superfamily. TE sites potentially under selection according to F_{ST} are flagged. (B) Location of the *Helitron* Ada TE insertion on chromosome 8 corresponding to its two closest genes. (C) Genomic niche of the *Helitron* Ada TE insertion on chromosome 8: F_{ST} values for each TE insertion, gene content (blue),

TE content (green) and GC-content (yellow). The grey section highlights TE loci with extremely differentiated population frequencies. (D) Number of Ada copies per isolate and population. (E) Phylogenetic trees of the coding sequences of each the MFS transporter upstream and the TATA box downstream of the TE insertion. Isolates of the two North American populations and an additional 11 isolates from other populations not carrying the insertion are shown. Blue color indicates TE presence, yellow indicates TE absence. (F) Frequency changes of the TE family Ada between the two North American populations compared to the other populations. Colors indicate the number of copies per chromosome. (G) Synteny plot of the Ada insertion locus on chromosome 8 between two complete genomes from the Middle East (TE missing) and North America (TE present). Figures S7-S11 show additional candidate regions.

Population-level expansions in TE content

If TE insertion dynamics are largely neutral across populations, TE frequencies across loci should reflect neutral population structure. To test this, we performed first a principal component analysis based on a set of six populations on four continents that represent the global genetic diversity of the pathogen (Figure 5A). The SNP set contained 900'193 genome-wide SNPs (Figure 5B). The population structure reflected the demographic history of the pathogen with clear continental differentiation and only minor within-site differentiation. In stark contrast, TE frequencies across loci showed only weak clustering by geographic origin with the Australian population being the most distinct (Figure 5D). We found a surprisingly strong differentiation of the two North American populations sampled at a 25-year interval in the same field in Oregon. To account for the lower number of TE loci, we performed an additional principal component analysis using a comparably sized SNP set to number of TE loci. Genome-wide SNPs retained the geographic signal of the broader set of SNPs (Figure 5C).

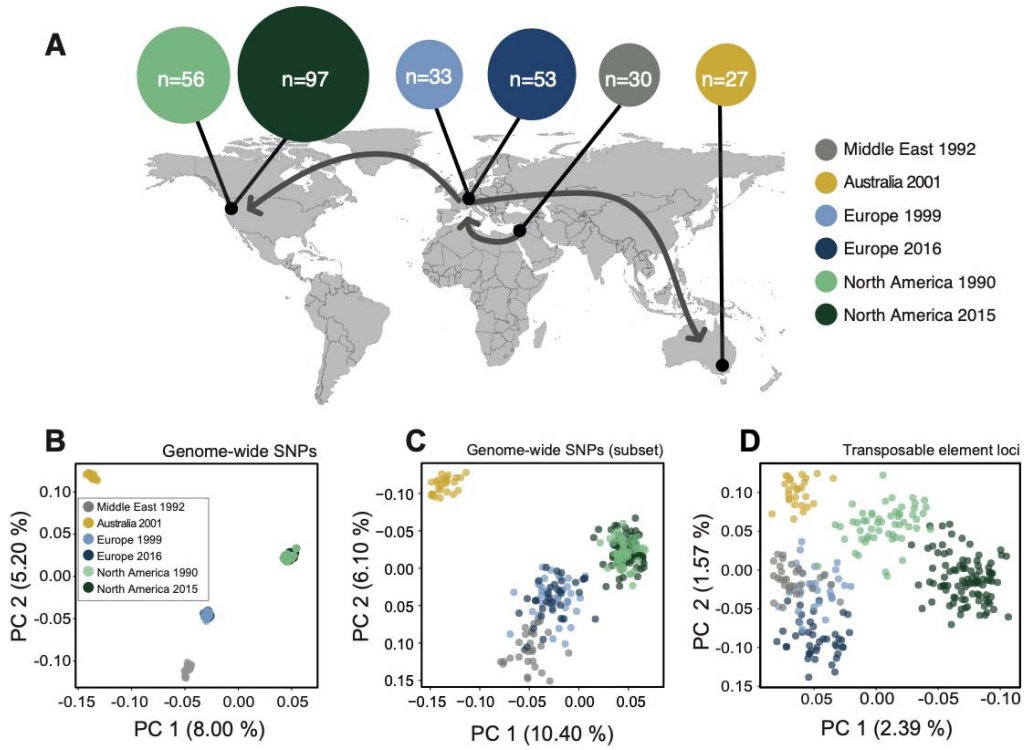

Figure 5: Population differentiation at transposable element (TE) and genome-wide SNP loci. (A) Sampling locations of the six populations. Middle East represents the region of origin of the pathogen. In North America, the two populations were collected at an interval of 25 years in the same field in Oregon. In Europe, two populations were collected at an interval of 17 years from two fields in Switzerland <20 km apart. Dark arrows indicate the historic colonization routes of the pathogen. (B) Principal component analysis (PCA) of 284 *Zymoseptoria tritici* isolates, based on 900'193 genome-wide SNPs. (C) PCA of a reduced SNP data set with randomly selected 203 SNPs matching approximately the number of analyzed TE loci. (D) PCA based on 193 TE insertion loci.

Unusual patterns in population differentiation at TE loci suggests that TE activity may drastically vary across populations (Figure 6A). To analyze this, we first identified the total TE content across all loci per isolate. We found generally low amounts of TEs in the Middle Eastern population from Israel (Figure 6B), which is close to the pathogen's center of origin (Stukenbrock *et al.*, 2007). Populations that underwent at least one migration bottleneck showed a substantial burst of TEs across all major superfamilies. These populations included the two populations from Europe (Switzerland) collected in 1999 and 2016 and the North American population from 1990, as well as the Australian population. We found a second stark increase in TE content in the North American population sampled in 2015 at the same site as the population from 1990. Strikingly, the isolate with

480 the lowest number of analyzed TEs collected in 2015 was comparable to the isolate with the highest
481 number of TEs at the same site in 1990. We tested whether sequencing coverage may explain
482 variation in the detected TEs across isolates, but we found no meaningful association
483 (Supplementary Figure S3B). We analyzed variation in TE copy numbers across families and found
484 that the expansions were mostly driven by *Gypsy* elements including the families Luna, Sol and
485 Venus, the *Copia* family Deimos and the LINE family Lucy (Figure 6C; Supplementary Figures S4-
486 6). We also found a burst specific to the two North American populations in *Helitron* elements
487 (Ada), an increase specific to Swiss populations in LINE elements, and an increase in *Copia*
488 elements in the Australian and the two North American populations. Analyses of complete *Z. tritici*
489 genomes from the same populations revealed high TE contents in Australia and North America
490 (Oregon 1990) (Badet et al. 2019). The complete genomes confirmed also that the increase in TEs
491 was driven by LINE, *Gypsy* and *Copia* families in Australia and *Helitron*, *Gypsy* and *Copia* families
492 in North America (Badet *et al.*, 2019).
493
494 Finally, we analyzed whether the population-specific expansions were accompanied by shifts in the
495 allele frequency spectra (Figure 6D). We found that the first step of expansions observed in
496 Australia and Europe were associated with a downwards shift in allele frequencies. This is consistent
497 with transposition activity creating new copies in the genomes and stronger purifying selection. In
498 contrast, the North American populations showed an upwards shift in allele frequencies indicating
499 relaxation of selection against TEs.
500

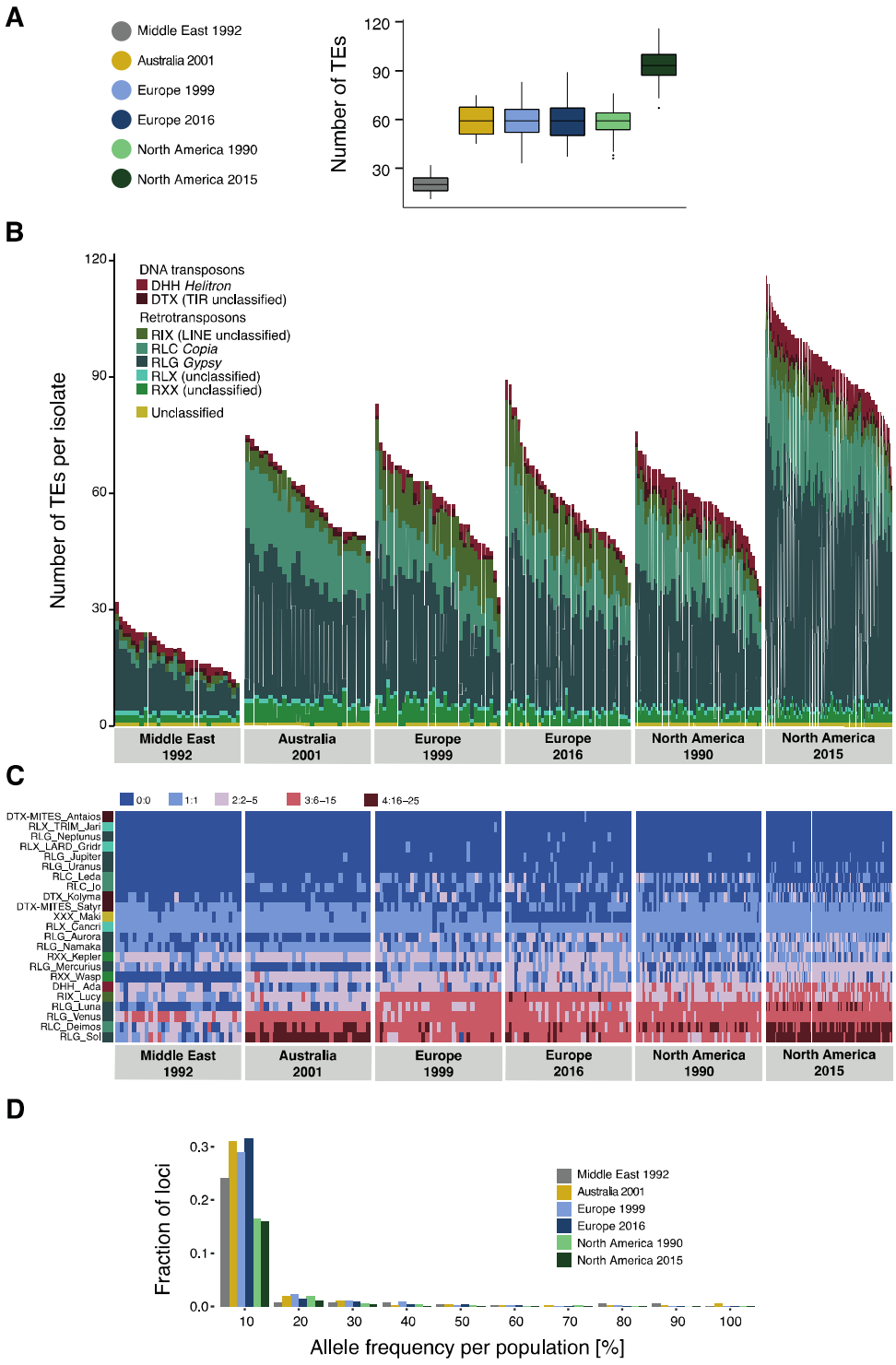

Figure 6: Global population structure of transposable element (TE) insertion polymorphism. (A) The number of transposable elements (TEs) per population. (C) Total TE copies per isolate. Colors stand identify TE superfamilies. (D) TE family copy numbers per isolate. (E) TE insertion frequency spectrum per population.

DISCUSSION

TEs play a crucial role in generating adaptive genetic variation within species but are also drivers of deleterious genome expansions. We analyzed the interplay of positive selection and incipient genome expansions using a large-scale population genomics dataset. TEs have substantial transposition activity in the genome but are strongly counter-selected and maintained at low frequency. TE dynamics showed distinct trajectories across populations with more recently established populations having higher TE content in the genome. This strongly suggests that population specific TE expansions are leading to changes in genome size. In parallel, individual TE loci possibly contributed to recent local adaptation related to fungicide resistance and host adaptation.

TRANSPOSITION ACTIVITY IS COUNTER-ACTED BY STRONG PURIFYING SELECTION

TE frequencies show a strong skew towards singleton TE insertions across the genome, consistent with transposition activity creating new insertions and purifying selection maintaining frequencies at a low level. This is a broadly-known pattern across plants and animals, including *Drosophila melanogaster*, *Zea mays*, *Brachypodium distachyon*, and *Arabidopsis thaliana* (Cridland *et al.*, 2013; Stuart *et al.*, 2016; Lai *et al.*, 2017; Stritt *et al.*, 2017). TE insertions were under-represented in or near coding regions, showing that purifying selection acts against TE insertions that disrupt genes. Coding sequences in the *Z. tritici* genome are densely spaced with an average distance of only ~ 1 kb (Goodwin *et al.*, 2011). Consistent with this high gene density, TE insertions close to genes peaked at a distance of 200-400 bp away from coding sequences. A rapid decay in linkage disequilibrium in the *Z. tritici* populations (Croll *et al.*, 2015; Hartmann *et al.*, 2018) likely contributed to the efficiency of removing deleterious insertions. The large number of low frequency insertion loci suggests that at least some TE families are transpositionally active and can create new copies. Analyses of sequence similarities and transcriptional activity suggest that several TE families are actively creating new copies in the *Z. tritici* genome (Dhillon *et al.*, 2014; Fouché *et al.*, 2019). The

transposition activity in a genome and counter-acting purifying selection is expected to establish an equilibrium over time (Charlesworth & Charlesworth, 1983). However, changes in population size due to bottlenecks or founder events are likely to shift the equilibrium. Furthermore, genetic drift may also impact the prevalence of active TEs or the fixation of mutations contributing to TE control.

TE INSERTIONS POTENTIALLY UNDERPINNING ADAPTIVE EVOLUTION IN POPULATIONS

An emerging theme across kingdoms is that a substantial fraction of adaptive genetic variation in populations is generated by the insertion of TEs (Chuong *et al.*, 2017). Population genomic datasets can be used to identify the most likely candidate loci underlying recent adaptation. The shallow genome-wide differentiation of *Z. tritici* populations provides a powerful background to test for outlier loci (Hartmann *et al.*, 2018). We focused on two scenarios for an adaptive TE insertion to arise across populations. We analyzed TE insertions to arise from a globally low frequency to a high frequency either in the most recent North American population or the most recent European population. The strongest candidate loci for TE-mediated adaptation were two TE insertions in close proximity to genes encoding major facilitator superfamily (MFS) transporters. For both loci, the frequency increase occurred in the North American populations which experienced the first systematic fungicide applications in the decade prior to the last sampling (Estep *et al.*, 2015). TE-mediated overexpression of the MFS1 transporter is a known resistance mechanism of *Z. tritici* and acts by increasing efflux of fungicides out of the cell (Omrane *et al.*, 2017). TE-mediated fungicide resistance adaptation in the North American population is further supported by a significant association of levels of fungicide resistance in the population and the presence of the *Gypsy* insertion near the MFS gene. Furthermore, the locus experienced a selective sweep following the insertion of the TE. We found that the same TEs experienced genome-wide copy number expansions, suggesting that the availability of adaptive TE insertions may be a by-product of a TE burst in individual populations.

POPULATION-LEVEL TE INVASIONS AND RELAXED SELECTION

Across the surveyed populations from four continents, we identified substantial variation in TE counts per individual. The increase in TEs matches the global colonization history established for *Z. tritici* (Zhan *et al.*, 2003; Stukenbrock *et al.*, 2007). Compared to the Israeli population located nearest the center of origin in the Middle East, the European populations showed a three-fold increase in TE counts. The Australian and North American populations established from European descendants retained high TE counts. We identified a second increase at the North American site where TE counts nearly doubled again over a 25-year period. Interestingly, the first TE expansion was caused by a broad increase in copy numbers across the spectrum of TE families. The second expansion at the North American site was driven by a small number of TE families. Analyses of completely assembled genomes from the same populations confirmed that genome expansions were primarily driven by *Gypsy*, *Copia* and *Helitron* superfamilies (Badet *et al.*, 2019). Consistent with the contributions from individual TEs, we found that the first expansion in Europe led to an increase in low-frequency variants, suggesting higher transposition activity of many TEs in conjunction with strong purifying selection. The second expansion at the North American site shifted TE frequencies upwards, suggesting relaxed selection against TEs. The population-level context of TEs in *Z. tritici* shows how heterogeneity in TE control interacts with demography to determine extant levels of TE content and, ultimately, genome size.

The activity of TEs is controlled by complex selection regimes within species. Actively transposing elements may accelerate genome evolution and underpin expansions. Hence, genomic defenses should evolve to efficiently target recently active TEs. Yet, TE-mediated adaptation involves selection favoring genotypes carrying active TEs, hence counteracting overall negative selection. In the case of *Z. tritici*, TE expansion activity and counteracting genomic defenses established a unstable equilibrium across the species range. Furthermore, we show that population subdivisions are at the origin of highly differentiated TE content within a species. The variability in TE content emerging over the span of only a few decades or centuries is largely sufficient to explain large

587 genome size expansion across deeper time scales and species. In conclusion, population-level
588 analyses can recapitulate incipient genome expansions driven by TEs.
589
590
591 **Acknowledgments**
592 We thank Andrea Sánchez Vallet, Anne Roulin and Luzia Stadler for helpful discussions and
593 comments on previous versions of the manuscript. DC is supported by the Swiss National Science
594 (grants 31003A_173265 and IZCOZO_177052) and the Fondation Pierre Mercier pour la Science.
595
596

REFERENCES

Andrews S, Lindenbaum P, Howard B, Ewels H. **2013**. FastQC: a quality control tool for high throughput sequence data.

Badet T, Oggenfuss U, Abraham L, Mcdonald BA, Croll D. **2019**. A 19-isolate reference-quality global pangenome for the fungal wheat pathogen Zymoseptoria tritici.

Bankevich A, Nurk S, Antipov D, Gurevich AA, Dvorkin M, Kulikov AS, Lesin VM, Nikolenko SI, Pham S, Prjibelski AD, *et al.* 2012. SPAdes: a new genome assembly algorithm and its applications to single-cell sequencing. *Journal of computational biology□: a journal of computational molecular cell biology* **19**: 455–77.

Bao W, Kojima KK, Kohany O. **2015**. Repbase Update, a database of repetitive elements in eukaryotic genomes. *Mobile DNA* **6**: 4–9.

Barnett DW, Garrison EK, Quinlan AR, Str□mberg MP, Marth GT. **2011**. Bamtools: A C++ API and toolkit for analyzing and managing BAM files. *Bioinformatics* **27**: 1691–1692.

Barron MG, Fiston-Lavier AS, Petrov DA, González J. **2014**. Population Genomics of Transposable Elements in Drosophila. In: Bassler BL, ed. Annual Review of Genetics, Vol 48. 561–581.

Blumenstiel JP, Chen X, He M, Bergman CM. **2014**. An age-of-allele test of neutrality for transposable element insertions. *Genetics* **196**: 523–538.

Bolger AM, Lohse M, Usadel B. **2014**. Trimmomatic: a flexible trimmer for Illumina sequence data. *Bioinformatics* **30**: 2114–2120.

Bonifacino JS, Glick BS. **2004**. The Mechanisms of Vesicle Budding and Fusion. *Cell* **116**: 153–166.

Butelli E, Licciardello C, Zhang Y, Liu J, Mackay S, Bailey P, Reforgiato-Recupero G, Martin C. **2012**. Retrotransposons control fruit-specific, cold-dependent accumulation of anthocyanins in blood oranges. *Plant Cell* **24**: 1242–1255.

Charlesworth B, Charlesworth D. **1983**. THE POPULATION-DYNAMICS OF TRANSPOSABLE ELEMENTS. *Genetical Research* **42**: 1–27.

Chuong EB, Elde NC, Feschotte C. **2017**. Regulatory activities of transposable elements: from conflicts to benefits. *Nature Reviews Genetics* **18**: 71–86.

Cridland JM, Macdonald SJ, Long AD, Thornton KR. **2013**. Abundance and distribution of transposable elements in two drosophila QTL mapping resources. *Molecular Biology and Evolution* **30**: 2311–2327.

Croll D, Lendenmann MH, Stewart E, McDonald BA. **2015**. The Impact of Recombination Hotspots on Genome Evolution of a Fungal Plant Pathogen. *Genetics* **201**: 1213-U787.

Croll D, Zala M, McDonald BA. **2013**. Breakage-fusion-bridge Cycles and Large Insertions Contribute to the Rapid Evolution of Accessory Chromosomes in a Fungal Pathogen. *Plos Genetics* **9**.

Darriba D, Taboada GL, Doallo R, Posada D. **2012**. jModelTest 2: more models, new heuristics and parallel computing. *Nature Methods* **9**: 772.

Dhillon B, Gill N, Hamelin RC, Goodwin SB. **2014**. The landscape of transposable elements in the finished genome of the fungal wheat pathogen Mycosphaerella graminicola. *Bmc Genomics* **15**.

Dobin A, Davis CA, Schlesinger F, Drenkow J, Zaleski C, Jha S, Gingeras TR, Batut P, Chaisson M. **2012**. STAR: ultrafast universal RNA-seq aligner. *Bioinformatics* **29**: 15–21.

Eichler EE, Sankoff D. **2003**. Structural dynamics of eukaryotic chromosome evolution. *Science* **301**: 793–797.

Estep LK, Torriani SFF, Zala M, Anderson NP, Flowers MD, Mcdonald BA, Mundt CC, Brunner PC. **2015**. Emergence and early evolution of fungicide resistance in North American populations of Zymoseptoria tritici. *Plant Pathology* **64**: 961–971.

Feschotte C. **2008**. Transposable elements and the evolution of regulatory networks. *Nature Reviews Genetics* **9**: 397–405.

Fouché S, Badet T, Oggenfuss U, Plissonneau C, Francisco CS, Croll D. **2019**. Stress-driven transposable element de-repression dynamics in a fungal pathogen. *Molecular Biology and Evolution*.

Frantzeskakis L, Kracher B, Kusch S, Yoshikawa-Maekawa M, Bauer S, Pedersen C, Spanu PD, Maekawa T, Schulze-Lefert P, Panstruga R. **2018**. Signatures of host specialization and a recent transposable element burst in the dynamic one-speed genome of the fungal barley powdery mildew pathogen. *BMC Genomics* **19**: 1–23.

Galagan JE, Selker EU. **2004**. RIP: the evolutionary cost of genome defense. *Trends in Genetics* **20**: 417–423.

Gautier M, Vitalis R. **2012**. Rehh An R package to detect footprints of selection in genome-wide SNP data from haplotype structure. *Bioinformatics* **28**: 1176–1177.

González J, Macpherson JM, Petrov DA. **2009**. A recent adaptive transposable element insertion near highly conserved developmental loci in Drosophila melanogaster. *Molecular Biology and Evolution* **26**: 1949–1961.

Goodwin SB, Ben M'Barek S, Dhillon B, Wittenberg AHJ, Crane CF, Hane JK, Foster AJ, Van der Lee TAJ, Grimwood J, Aerts A, *et al.* 2011. Finished Genome of the Fungal Wheat Pathogen Mycosphaerella graminicola Reveals Dispensome Structure, Chromosome Plasticity, and Stealth Pathogenesis. *Plos Genetics* **7**.

Goudet J, Jombart T. **2015**. Estimation and Tests of Hierarchical F-Statistics. R package version 0.04-22.

Grandaubert J, Bhattacharyya A, Stukenbrock EH. **2015**. RNA-seq-Based Gene Annotation and Comparative Genomics of Four Fungal Grass Pathogens in the Genus Zymoseptoria Identify Novel Orphan Genes and Species-Specific Invasions of Transposable Elements. *G3-Genes Genomes Genetics* **5**: 1323–1333.

Guindon S, Dufayard J-F, Lefort V, Anisimova M, Hordijk W, Gascuel O. **2010**. New Algorithms and Methods to Estimate Maximum-Likelihood Phylogenies: Assessing the Performance of PhyML 3.0. *Systematic Biology* **59**: 307–321.

Guindon S, Gascuel O. **2003**. A simple, fast, and accurate algorithm to estimate large phylogenies by maximum likelihood. *Systematic Biology* **52**: 696–704.

Guy L, Kultima JR, Andersson SGE. **2010**. GenoPlotR: comparative gene and genome visualization in R. *Bioinformatics* **26**: 2334–2335.

Hartmann F, Croll D. **2017**. Distinct Trajectories of Massive Recent Gene Gains and Losses in Populations of a Microbial Eukaryotic Pathogen. *Molecular Biology and Evolution.*

Hartmann F, McDonald M, Croll D. **2018**. Genome-wide evidence for divergent selection between populations of a major agricultural pathogen. *Molecular Ecology* **27**: 2725–2741.

Hartmann F, Sanchez-Vallet A, McDonald B, Croll D. **2017**. A fungal wheat pathogen evolved host specialization by extensive chromosomal rearrangements. *ISME J*.

Hollister JD, Gaut BS. **2009**. Epigenetic silencing of transposable elements: A trade-off between reduced transposition and deleterious effects on neighboring gene expression. *Genome Research* **19**: 1419–1428.

Huson DH, Richter DC, Rausch C, Dezulian T, Franz M, Rupp R. **2007**. Dendroscope: An interactive viewer for large phylogenetic trees. *BMC Bioinformatics* **8**: 1–6.

Jiao W-B, Schneeberger K. **2019**. Chromosome-level assemblies of multiple Arabidopsis thaliana accessions reveal hotspots of genomic rearrangements. *bioRxiv*: 738880.

Jombart T. **2008**. Adegenet: A R package for the multivariate analysis of genetic markers. *Bioinformatics* **24**: 1403–1405.

Jombart T, Ahmed I. **2011**. adegenet 1.3-1: New tools for the analysis of genome-wide SNP data. *Bioinformatics* **27**: 3070–3071.

Jurka J, Bao W, Kojima KK. **2011**. Families of transposable elements, population structure and the origin of species. *Biology Direct* **6**: 44.

Katoh K, Standley DM. **2013**. MAFFT multiple sequence alignment software version 7: Improvements in performance and usability. *Molecular Biology and Evolution* **30**: 772–780.

Kidwell MG. **2002**. Transposable elements and the evolution of genome size in eukaryotes. *Genetica* **115**: 49–63.

Krishnan P, Meile L, Plissonneau C, Ma X, Hartmann FE, Croll D, McDonald BA, Sánchez-Vallet A. **2018**. Transposable element insertions shape gene regulation and melanin production in a fungal pathogen of wheat. *BMC Biology* **16**: 1–18.

Lai X, Schnable JC, Liao Z, Xu J, Zhang G, Li C, Hu E, Rong T, Xu Y, Lu Y. **2017**. Genome-wide characterization of non-reference transposable element insertion polymorphisms reveals genetic diversity in tropical and temperate maize. *BMC Genomics* **18**: 1–13.

Langmead B, Salzberg SL. **2012**. Fast gapped-read alignment with Bowtie 2. *Nature Methods* **9**: 357–359.

Lawrence M, Huber W, Pagès H, Aboyoun P, Carlson M, Gentleman R, Morgan MT, Carey VJ. **2013**. Software for Computing and Annotating Genomic Ranges. *PLoS Computational Biology* **9**: 1–10.

Li H, Durbin R. **2009**. Fast and accurate short read alignment with Burrows-Wheeler transform. *Bioinformatics* **25**: 1754–1760.

Li H, Handsaker B, Wysoker A, Fennell T, Ruan J, Homer N, Marth G, Abecasis G, Durbin R. **2009**. The Sequence Alignment/Map format and SAMtools. *Bioinformatics* **25**: 2078–2079.

Lim JK. **1988**. Intrachromosomal rearrangements mediated by hobo transposons in Drosophila melanogaster. *PNAS* **85**: 9153–9157.

Linde CC, Zhan J, McDonald BA. **2002**. Population Structure of *Mycosphaerella graminicola*□: From Lesions to Continents. *Phytopathology* **92**: 946–955.

Linheiro RS, Bergman CM. **2012**. Whole Genome Resequencing Reveals Natural Target Site Preferences of Transposable Elements in Drosophila melanogaster. *PLOS ONE* **7**.

Lu L, Chen J, Robb SMC, Okumoto Y, Stajich JE, Wessler SR. **2017**. Tracking the genome-wide outcomes of a transposable element burst over decades of amplification. *Proceedings of the National Academy of Sciences*: 201716459.

Lynch M. **2007**. *The Origins of genome architecture*. Sunderland MA: Sinauer Associates.

McDonald BA, Mundt CC, Chen R. **1996**. The role of selection on the genetic structure of pathogen populations□: Evidence from field experiments with Mycosphaerella graminicola on wheat. : 73–80.

McKenna A, Hanna M, Banks E, Sivachenko A, Cibulskis K, Kernytsky A, Garimella K, Altshuler D, Gabriel S, Daly M, *et al.* 2010. The Genome Analysis Toolkit: A MapReduce framework for analyzing next-generation DNA sequencing data. *Genome Research* **20**: 1297–1303.

Meile L, Croll D, Brunner PC, Plissonneau C, Hartmann FE, Mcdonald BA, Sánchez-Vallet A. **2018**. A fungal avirulence factor encoded in a highly plastic genomic region triggers partial resistance to septoria tritici blotch. *New Phytologist*.

Nelson MG, Linheiro RS, Bergman CM. **2017**. McClintock: An Integrated Pipeline for Detecting Transposable Element Insertions in Whole-Genome Shotgun Sequencing Data. *G3: Genes|Genomes|Genetics* **7**: 2763–2778.

Odorizzi G, Babst M, Emr SD. **2000**. Phosphoinositide signaling and the regulation of membrane trafficking in yeast. *Trends in Biochemical Sciences* **25**: 229–235.

Oliver KR, McComb JA, Greene WK. **2013**. Transposable elements: Powerful contributors to angiosperm evolution and diversity. *Genome Biology and Evolution* **5**: 1886–1901.

Omrane S, Audéon C, Ignace A, Duplaix C, Aouini L, Kema G, Walker A-S, Fillinger S. **2017**. Plasticity of the MFS1 promoter leads to multi drug resistance in the wheat pathogen Zymoseptoria tritici. *mSphere*: 1–42.

Omrane S, Sghyer H, Audeon C, Lanen C, Duplaix C, Walker AS, Fillinger S. **2015**. Fungicide efflux and the MgMFS1 transporter contribute to the multidrug resistance phenotype in Zymoseptoria tritici field isolates. *Environmental Microbiology* **17**: 2805–2823.

Peter M, Kohler A, Ohm RA, Kuo A, Krutzmann J, Morin E, Arend M, Barry KW, Binder M, Choi C, *et al.* 2016. Ectomycorrhizal ecology is imprinted in the genome of the dominant symbiotic fungus Cenococcum geophilum. *Nature Communications* **7**.

Petrov DA, Aminetzach YT, Davis JC, Bensasson D, Hirsh AE. **2003**. Size matters: Non-LTR retrotransposable elements and ectopic recombination in Drosophila. *Molecular Biology and Evolution* **20**: 880–892.

Plissonneau C, Sturchler A, Croll D. **2016**. The Evolution of Orphan Regions in Genomes of a Fungal Pathogen of Wheat. *Mbio* **7**.

Quinlan AR, Hall IM. **2010**. BEDTools: A flexible suite of utilities for comparing genomic features. *Bioinformatics* **26**: 841–842.

R Core Team. **2017**. R: A language and environment for statistical computing. R Foundation for Statistical Computing, Vienna, Austria.

Raffaele S, Kamoun S. **2012**. Genome evolution in filamentous plant pathogens: why bigger can be better. *Nature Reviews Microbiology* **10**: 417–430.

Rice P, Longden L, Bleasby A. **2000**. EMBOSS: The European Molecular Biology Open Software Suite. *Trends in Genetics* **16**: 276–277.

Ritz C, Streibig JC. **2005**. Bioassay analysis using R. *Journal of Statistical Software* **12**: 1–22.

Rizzon C, Martin E, Marais G, Duret L, Ségalat L, Biémont C. **2003**. Patterns of Selection Against Transposons Inferred from the Distribution of Tc1, Tc3 and Tc5 Insertions in the mut-7 Line of the Nematode Caenorhabditis elegans. *Genetics* **165**: 1127–1135.

Rouxel T, Grandaubert J, Hane JK, Hoede C, van de Wouw AP, Couloux A, Dominguez V, Anthouard V, Bally P, Bourras S, *et al.* 2011. Effector diversification within compartments of the Leptosphaeria maculans genome affected by Repeat-Induced Point mutations. *Nature communications* **2**: 202.

Sabeti PC, Varilly P, Fry B, Lohmueller J, Hostetter E, Cotsapas C, Xie X, Byrne EH, McCarroll SA, Gaudet R, *et al.* 2007. Genome-wide detection and characterization of positive selection in human populations. *Nature* **449**: 913–918.

SanMiguel P, Gaut BS, Tikhonov A, Nakajima Y, Bennetzen JL. **1998**. The paleontology of intergene retrotransposons of maize. *Nature Genetics* **20**: 43–45.

Shen RM, Batzer MA, Deininger PL. **1991**. Evolution of the master Alu gene(s). *Journal of Molecular Evolution* **33**: 311–320.

Slotkin RK, Martienssen R. **2007**. Transposable elements and the epigenetic regulation of the genome. *Nature Reviews Genetics* **8**: 272–285.

Smit A, Hubley R. RepeatModeler Open-1.0.

Stöver BC, Müller KF. **2010**. TreeGraph 2: Combining and visualizing evidence from different phylogenetic analyses. *BMC Bioinformatics* **11**: 1–9.

Stritt C, Gordon SP, Wicker T, Vogel JP, Roulin AC. **2017**. Recent activity in expanding populations and purifying selection have shaped transposable element landscapes across natural accessions of the Mediterranean grass Brachypodium distachyon. *Genome Biology and Evolution* **10**: 1–38.

Stuart T, Eichten SR, Cahn J, Karpievitch Y V, Borevitz JO, Lister R. **2016**. Population scale mapping of transposable element diversity reveals links to gene regulation and epigenomic variation. *Elife* **5**.

Stukenbrock EH, Banke S, Javan-Nikkhah M, McDonald BA. **2007**. Origin and domestication of the fungal wheat pathogen Mycosphaerella graminicola via sympatric speciation. *Molecular Biology and Evolution* **24**: 398–411.

van't Hof AE, Campagne P, Rigden DJ, Yung CJ, Lingley J, Quail MA, Hall N, Darby AC,

Saccheri IJ. **2016**. The industrial melanism mutation in British peppered moths is a transposable element. *Nature* **534**: 102–105.

Walser J-C, Chen B, Feder ME. **2006**. Heat-Shock Promoters: Targets for Evolution by P Transposable Elements in Drosophila. *PLoS Genetics* **2**: e165.

Waterhouse AM, Procter JB, Martin DMA, Clamp M, Barton GJ. **2009**. Jalview Version 2-A multiple sequence alignment editor and analysis workbench. *Bioinformatics* **25**: 1189–1191.

Wickham H. **2016**. *ggplot2: Elegant Graphics for Data Analysis*. New York: Springer-Verlag.

Wickham H, Chang W. **2016**. devtools: Tools to Make Developing R Packages Easier.

Wickham H, Francois R, Henry L, Müller K. **2017**. dplyr: A Grammar of Data Manipulation.

Wong WY, Simakov O, Bridge DM, Cartwright P, Bellantuono AJ, Kuhn A, Holstein TW, David CN, Steele RE, Martínez DE. **2019**. Expansion of a single transposable element family is associated with genome-size increase and radiation in the genus Hydra. *PNAS*: 1–3.

Zhan J, Kema GHJ, Waalwijk C, McDonald BA. **2002**. Distribution of mating type alleles in the wheat pathogen Mycosphaerella graminicola over spatial scales from lesions to continents. *Fungal Genetics and Biology* **36**: 128–136.

Zhan J, Linde CC, Jurgens T, Merz U, Steinebrunner F, McDonald BA. **2005**. Variation for neutral markers is correlated with variation for quantitative traits in the plant pathogenic fungus Mycosphaerella graminicola. *Mol Ecol* **14**: 2683–2693.

Zhan J, Pettway RE, McDonald BA. **2003**. The global genetic structure of the wheat pathogen Mycosphaerella graminicola is characterized by high nuclear diversity, low mitochondrial diversity, regular recombination, and gene flow. *Fungal Genetics and Biology* **38**: 286–297.

Zhang L, Hu J, Han X, Li J, Gao Y, Richards CM, Zhang C, Tian Y, Liu G, Gul H, *et al.* 2019. A high-quality apple genome assembly reveals the association of a retrotransposon and red fruit colour. *Nature Communications* **10**: 1494.

Zheng X, Gogarten SM, Lawrence M, Stilp A, Conomos MP, Weir BS, Laurie C, Levine D. **2017**. SeqArray-a storage-efficient high-performance data format for WGS variant calls. *Bioinformatics* **33**: 2251–2257.

Zheng X, Levine D, Shen J, Gogarten SM, Laurie C, Weir BS. **2012**. A high-performance computing toolset for relatedness and principal component analysis of SNP data. *Bioinformatics* **28**: 3326–3328.